Journal of Solid State Chemistry 184 (2011) 241–245

Contents lists available at ScienceDirect

Journal of Solid State Chemistry

journal homepage: www.elsevier.com/locate/jssc

Heat capacity, enthalpy and entropy of ternary bismuth tantalum oxides

J. Leitner [a,*], V. Jakeš [b], Z. Sofer [b], D. Sedmidubský [b], K. Růžička [c], P. Svoboda [d]

[a] Department of Solid State Engineering, Institute of Chemical Technology Prague, Technická 5, 166 28 Prague 6, Czech Republic
[b] Department of Inorganic Chemistry, Institute of Chemical Technology Prague, Technická 5, 166 28 Prague 6, Czech Republic
[c] Department of Physical Chemistry, Institute of Chemical Technology Prague, Technická 5, 166 28 Prague 6, Czech Republic
[d] Department of Condensed Matter Physics, Faculty of Mathematics and Physics, Charles University, Ke Karlovu 5, 121 16 Prague 2, Czech Republic

ARTICLE INFO

Article history:
Received 14 September 2010
Received in revised form
11 November 2010
Accepted 16 November 2010
Available online 20 November 2010

Keywords:
Enthalpy increments
Heat capacity
Entropy
Calorimetry
Bismuth tantalum oxide
Bismuth tantalate

ABSTRACT

Heat capacity and enthalpy increments of ternary bismuth tantalum oxides $Bi_4Ta_2O_{11}$, $Bi_7Ta_3O_{18}$ and Bi_3TaO_7 were measured by the relaxation time method (2–280 K), DSC (265–353 K) and drop calorimetry (622–1322 K). Temperature dependencies of the molar heat capacity in the form $C_{pm}=445.8+0.005451T-7.489\times10^6/T^2$ J K^{-1} mol^{-1}, $C_{pm}=699.0+0.05276T-9.956\times10^6/T^2$ J K^{-1} mol^{-1} and $C_{pm}=251.6+0.06705T-3.237\times10^6/T^2$ J K^{-1} mol^{-1} for Bi_3TaO_7, $Bi_4Ta_2O_{11}$ and for $Bi_7Ta_3O_{18}$, respectively, were derived by the least-squares method from the experimental data. The molar entropies at 298.15 K, $S^\circ_m(298.15\text{ K})=449.6\pm2.3$ J K^{-1} mol^{-1} for $Bi_4Ta_2O_{11}$, $S^\circ_m(298.15\text{ K})=743.0\pm3.8$ J K^{-1} mol^{-1} for $Bi_7Ta_3O_{18}$ and $S^\circ_m(298.15\text{ K})=304.3\pm1.6$ J K^{-1} mol^{-1} for Bi_3TaO_7, were evaluated from the low-temperature heat capacity measurements.

1. Introduction

Ternary bismuth tantalum oxides (bismuth tantalates) are of considerable interest because they are constituents of practically important ternary systems $SrO–Bi_2O_3–Ta_2O_5$ and $Bi_2O_3–Ta_2O_5–Nb_2O_5$. Ternary oxide $SrBi_2Ta_2O_9$ is one of the most promising candidates for lead-free non-volatile random access memory applications while solid solutions $Bi(Ta,Nb)O_4$ and $Bi_3(Ta,Nb)O_7$ have found some technological applications such as microwave dielectrics or photocatalysts.

Phase relations in the Bi-rich part of binary system $Bi_2O_3–Ta_2O_5$ have been studied by Zhou [1,2] and Ling et al. [3–6]. Using X-ray diffraction, selected area electron diffraction and high-resolution electron microscopy Zhou [2] identified a number of phases: tetragonal $(Bi,Ta)O_x$ solid solution, δ-Bi_2O_3 based cubic $(Bi,Ta)O_y$ solid solution in the composition range $Bi_{19}TaO_{31}–B_3TaO_7$ and four stoichiometric ternary oxides $Bi_7Ta_3O_{18}$, $Bi_4Ta_2O_{11}$, $Bi_{31}Ta_{17}O_{89}$ and $BiTaO_4$. Atomic arrangements in these crystalline phases are rather complicated and superstructures of different symmetry were recognized. Similar findings were presented by Ling et al. [3,6] based on the X-ray diffraction and electron diffraction data. A refinement of the crystal structure of $Bi_7Ta_3O_{18}$ was performed later [4] using single-crystal X-ray diffraction and powder neutron diffraction data. A triclinic ($P1$) crystal structure was assigned to $Bi_7Ta_3O_{18}$ however a monoclinic ($C2/m$) crystal structure reproduced the experimental data comparably well. A triclinic ($P-1$) crystal structure was proposed for $Bi_4Ta_2O_{11}$ [5] based on synchrotron X-ray diffraction and powder neutron diffraction data. Crystal structure of Bi_3TaO_7 was examined by X-ray and neutron powder diffraction by Abrahams et al. [7]. This oxide possesses a defect fluorite structure (Fm-$3m$). $BiTaO_4$ is known to exist in low-temperature (LT) orthorhombic structure and high-temperature (HT) triclinic structure [8–10]. The temperature of equilibrium transformation LT↔HT is not known but according to conditions used for the preparation of LT and HT modifications it falls into 1073–1173 K interval.

There is only one report [11] dealing with thermodynamic properties of Bi–Ta ternary oxides. Hampl et al. measured the heat capacity (2–570 K) and enthalpy increments (670–1170 K) of polycrystalline $BiTaO_4$ LT modification. The value of standard molar entropy at 298.15 K $S_m(298.15\text{ K})=149.11$ J K^{-1} mol^{-1} was evaluated from low-temperature dependence of $C_{pm}(T)$. The aim of this work is the measurement of the heat capacity and enthalpy increments of bismuth tantalates $Bi_4Ta_2O_{11}$, $Bi_7Ta_3O_{18}$ and Bi_3TaO_7 in a broad temperature range and evaluation of the standard molar entropy of these ternary oxides at 298.15 K, as well as the temperature dependence of C_{pm} above room temperature.

2. Experimental

The samples were prepared by conventional solid state reactions from high purity Bi_2O_3 (99.9%, Aldrich) and Ta_2O_5 (99.85%,

* Corresponding author. Fax: +420 220 444 330.
E-mail address: Jindrich.Leitner@vscht.cz (J. Leitner).

0022-4596/$ - see front matter © 2010 Elsevier Inc. All rights reserved.
doi:10.1016/j.jssc.2010.11.020

Alfa Aesar). The stoichiometric amounts of precursors were ground in agate mortar, pressed into pellets and fired at 1073 K in platinum crucible in air atmosphere for 48 h. After regrinding the pellets, the coarse powder was ball milled for 30 min at 500 rpm, pressed again and fired at 1103 K in air for 100 h. Phase composition of the prepared samples was checked by the X-ray powder diffraction (XRD). XRD data were collected at room temperature with an X'Pert PRO (PANalytical, the Netherlands) $\theta-\theta$ powder diffractometer with parafocusing Bragg–Brentano geometry using Cu$K\alpha$ radiation ($\lambda=1.5418$ Å, $U=40$ kV, $I=30$ mA). Data were scanned over the angular range $5-60^\circ$ (2θ) with an increment of 0.02° (2θ) and a counting time of 0.3 s step^{-1}. Data evaluation was performed by means of the HighScore Plus software package. To exclude a potential contamination of the prepared samples with Pt as a result of Bi_2O_3 attack of crucible material at high temperatures the samples chemical composition was checked by X-ray fluorescent analysis (Axios, PANalytical, the Netherlands).

The PPMS equipment 14T-type (Quantum Design, USA) was used for the heat capacity measurements in the low-temperature region [12–16]. The measurements were performed by the relaxation method [17] with fully automatic procedure under high vacuum (pressure $\sim10^{-2}$ Pa) to avoid heat loss through the exchange gas. The samples were compressed into powder plates of approx. 4.4–12.6 mg. The densities of the pressed samples were about 65% of the theoretical ones. The samples were mounted to the calorimeter platform with cryogenic grease Apiezon N (supplied by Quantum Design). The procedure was as follows: First, a blank sample holder with the Apiezon only was measured in the temperature range approx. 2–280 K to obtain background data, then the sample plate was attached to the calorimeter platform and the measurement was repeated in the same temperature range with the same temperature steps. The sample heat capacity was then obtained as a difference between the two datasets. This procedure was applied, because the heat capacity of Apiezon is not negligible in comparison with the sample heat capacity ($\sim$8% at room temperature) and exhibits a sol–gel transition below room temperature [18].

The manufacturer claims the precision of this measurement is better than 2% [19]; the control measurement of the copper sample (99.999% purity) confirmed this precision in the temperature range 50–250 K. However, the precision of the measurement strongly depends on the thermal coupling between the sample and the calorimeter platform. Due to unavoidable porosity of the sample plate this coupling is rapidly getting worse as the temperature raises above 270 K and Apiezon diffuses into the porous sample. Consequently, the uncertainty of the obtained data tends to be larger.

A Micro DSC III calorimeter (Setaram, France) in the incremental temperature scanning mode consisting of a number of 5–10 K steps (heating rate 0.2 K min^{-1}) followed by isothermal delays of 9000 s was used for the heat capacity determination in the temperature range 265–353 K. Synthetic sapphire, NIST Standard reference material No. 720, was used as the reference. The typical sample mass was 2.5–3.5 g. The uncertainty of heat capacity measurements is estimated to be better than ±1%.

Enthalpy increment determinations were carried out by drop method using high-temperature calorimeter, Multi HTC 96 (Setaram, France). All measurements were performed in air by alternating dropping of the reference material (small pieces of synthetic sapphire, NIST Standard reference material No. 720) and of the sample (pressed pellets 5 mm in diameter) being initially held at room temperature, through a lock into the working cell of the preheated calorimeter. Endothermic effects are detected and the relevant peak area is proportional to the heat content of the dropped specimen. The measurements were performed at temperatures 622–1322 K on samples of 240–390 mg. The delays between two subsequent drops were 25–30 min. To check the accuracy of measurement, the enthalpy increments of platinum in the temperature range 770–1370 K were measured first and compared with published reference values [20]. The standard deviation of 22 runs was 0.47 kJ mol^{-1}, the average relative error was 2.0%. Estimated overall accuracy of the drop measurements is ±3%.

3. Results and discussion

The XRD analysis revealed that the prepared samples were without any observable diffraction lines from unreacted precursors or other phases (see the Supplementary Figs. S1–S3). The lattice parameters of the oxides were evaluated by Rietveld refinement [21] and are summarized in Table 1. Using the XRF analysis any Pt contamination exceeding $\approx10^{-2}$ wt% was ruled out.

The measured data used for further analysis for $Bi_4Ta_2O_{11}$ involve 187 C_{pm} values from relaxation time (2.3–267 K), 36 points from DSC (266–353 K) and 48 values of the enthalpy increments from the drop measurements (622–1271 K). For $Bi_7Ta_3O_{18}$, 88 C_{pm} values from relaxation time (1.8–259.1 K), 36 points from DSC (266–353 K) and 29 values of the enthalpy increments from the drop measurement (672–1322 K) were obtained. Finally, 103 C_{pm} values from relaxation time (1.9–287.5 K), 36 points from DSC (266–353 K) and 42 values of the enthalpy increments from the drop measurement (623–1271 K) were obtained for Bi_3TaO_7. All C_{pm} data are plotted in Fig. 1 and summarized in Supplementary Tables S1 and S2. Enthalpy increment data are shown in Fig. 2 and listed in Supplementary Table S3.

The fit of the low-temperature heat capacity data (LT fit) consists of two steps. Assuming the validity of the phenomenological formula $C_{pm}=\beta T^3+\gamma_{el}T$, at $T\to0$ where β is proportional to the Debye temperature Θ_D and $\gamma_{el}T$ is the Sommerfeld term, we plotted the C_{pm}/T vs. T^2 dependence for $T<8$ K. The non-zero γ_{el} values (probably

Table 1
Crystal structures, lattice parameters and densities of prepared powder samples.

Oxide	$Bi_4Ta_2O_{11}$		$Bi_7Ta_3O_{18}$		Bi_3TaO_7	
	This work	01-089-4353[a]	This work	01-089-6647[a]	This work	00-044-0202[a]
Space group	*P*-1	*P*-1	*C*2/*m*	*C*2/*m*	*Fm*-3*m*	*Fm*-3*m*
a (nm)	0.66159	0.66089	3.40162	3.40084	0.54593	0.54711
b (nm)	0.76528	0.76569	0.76054	0.76069	0.54593	0.54711
c (nm)	0.98781	0.98828	0.66354	0.66364	0.54593	0.54711
α (deg.)	101.3926	101.3450	90.0	90.0	90.0	90.0
β (deg.)	90.0993	90.1830	109.1606	109.2380	90.0	90.0
γ (deg.)	89.9921	90.0290	90.0	90.0	90.0	90.0
d (g cm^{-3})[b]	9.39	9.30	9.47	9.40	9.39	9.32

[a] JCPDS reference code.
[b] Theoretical density calculated from the lattice parameters.

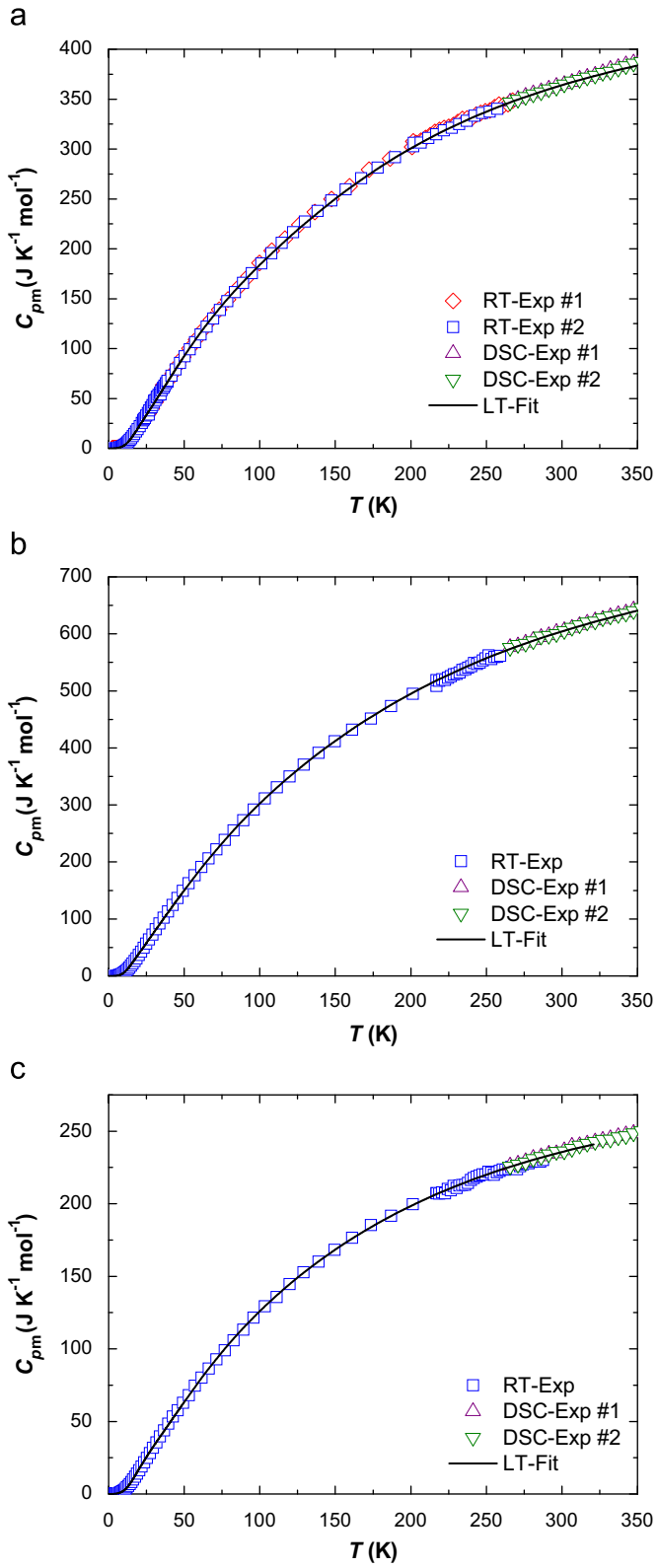

Fig. 1. Low-temperature heat capacity of $Bi_4Ta_2O_{11}$ (a), $Bi_7Ta_3O_{18}$ (b) and Bi_3TaO_7 (c).

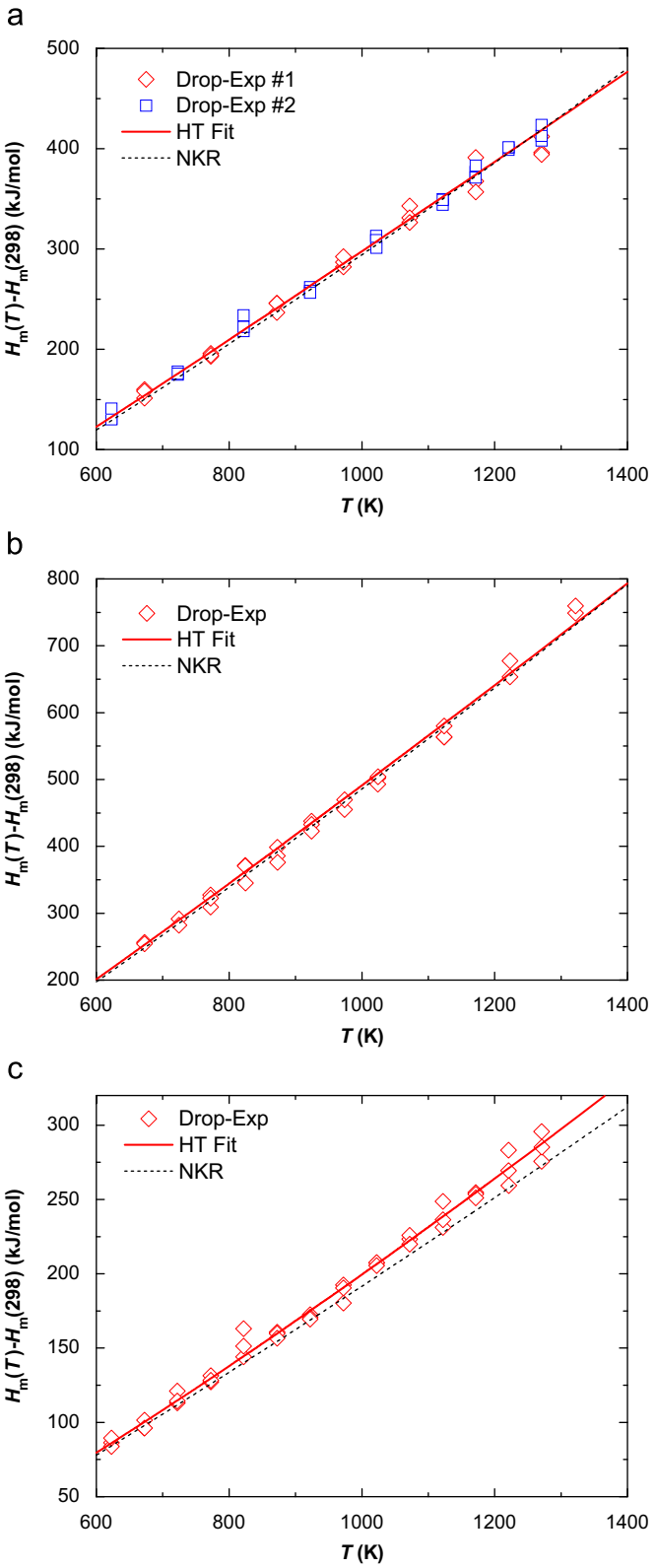

Fig. 2. Enthalpy increments of $Bi_4Ta_2O_{11}$ (a), $Bi_7Ta_3O_{18}$ (b) and Bi_3TaO_7 (c).

due to some metallic impurities or a series of Schottky-like transitions due to structure defects) are negligible in all cases ($\sim$0.5 mJ K^{-1} mol^{-1}) and can be ignored in further analysis. Simultaneously, the C_{pm}/T vs. T^2 plot provides an estimation of Θ_D, as in this temperature range only the acoustic phonons are populated.

In the second step of the LT fit, both sets of the C_{pm} data (relaxation time+DSC) were considered. Analysis of the phonon heat capacity was performed as an additive combination of Debye and Einstein models. The phonon spectrum of a polyatomic compound contains three acoustic branches and $3n$–3 optical ones,

where n is number of atoms per formula unit. In our case, i.e. 17 ($Bi_4Ta_2O_{11}$), 28 ($Bi_7Ta_3O_{18}$) and 11 (Bi_3TaO_7) atoms/f.u., this represents 48, 81 and 30 optical branches, respectively. (Let us note that this approach is still a simplification, since n should properly refer to the number of atoms per primitive unit cell.) However, this would lead to an inadequate increase of parameters to be fitted. To reduce the number of adjustable parameters, several individual branches are grouped together into multiple degenerate branches with the same characteristic temperatures using a trial-and-error method.

Both models include corrections for anharmonicity, which is responsible for a small, but not negligible, additive term at higher temperatures and which accounts for the discrepancy between isobaric and isochoric heat capacity. According to literature [22], the term $1/(1-\alpha T)$ is considered as a correction factor.

The acoustic part of the phonon heat capacity is then described using the Debye model in the form

$$C_{\mathrm{phD}} = \frac{9R}{1-\alpha_{\mathrm{D}}T}\left(\frac{T}{\Theta_{\mathrm{D}}}\right)^3 \int_0^{x_D} \frac{x^4\exp(x)}{[\exp(x)-1]^2}\,\mathrm{d}x \quad (1)$$

where R is the gas constant, Θ_{D} is the Debye characteristic temperature, α_{D} is the coefficient of anharmonicity of acoustic branches and $x_{\mathrm{D}}=\Theta_{\mathrm{D}}/T$. Here the three acoustic branches are taken as one triply degenerate branch. Similarly, the individual optical branches are described by the Einstein model

$$C_{\mathrm{phE}i} = \frac{R}{1-\alpha_{\mathrm{E}i}T}x_{\mathrm{E}i}^2\frac{\exp(x_{\mathrm{E}i})}{[\exp(x_{\mathrm{E}i})-1]^2} \quad (2)$$

where $\alpha_{\mathrm{E}i}$ and $x_{\mathrm{E}i}=\Theta_{\mathrm{E}i}/T$ have analogous meanings as in the previous case. Several optical branches are again grouped into one degenerate multiple branch with the same Einstein characteristic temperature and anharmonicity coefficient. The phonon heat capacity then reads

$$C_{\mathrm{ph}} = C_{\mathrm{phD}} + \sum_{i=1}^{3n-3} C_{\mathrm{phE}i} \quad (3)$$

All the estimated values were included into the simplex routine [23] and a full non-linear fit was performed on all adjustable parameters. The analysis of the phonon heat capacity is summarized in Table 2.

The values of relative enthalpies at 298.15 K, $H_{\mathrm{m}}(298.15)-H_{\mathrm{m}}(0)$, for ternary bismuth tantalum oxides were evaluated from the low-temperature C_{pm} data (LT fit) by numerical integration of the $C_{\mathrm{pm}}(T)$ dependences from zero to 298.15 K. Standard deviations (2σ) were calculated using the error propagation law. The values of standard molar entropies at 298.15 K, $S_{\mathrm{m}}(298.15)$, were derived from the low-temperature C_{pm} data (LT fit) by numerical integration of the $C_{pm}(T)/T$ dependences from zero to 298.15 K. A numerical integration was used with the boundary conditions $S_{\mathrm{m}}=0$ and $C_{pm}/T=\gamma_{\mathrm{el}}$ at $T=0$ K. Standard deviations (2σ) were calculated using the error propagation law. All calculated values are summarized in Table 3.

For the assessment of temperature dependencies C_{pm} above room temperature, the heat capacity data from DSC and the enthalpy increment data from drop calorimetry were treated simultaneously (HT fit). Different weights w_i were assigned to individual points calculated as $w_i=1/\delta_i^2$ where δ_i is the absolute deviation of the ith measurement estimated from overall accuracies of the measurements (1% for DSC and 3% for drop calorimetry). Both types of experimental data thus gain comparable significance during the regression analysis. To smoothly connect the LT fit and HT fit data the values of $C_{pm}(298.15)$ from LT fit (see Table 3) were used as constraints. The temperature dependencies of the heat capacities of the investigated bismuth tantalates (T=298.15–1400 K) can thus be expressed by

$Bi_4Ta_2O_{11}$

$$C_{pm} = (445.8\pm18.2)+(5.451\pm23.344)\times10^{-3}T - \frac{(7.489\pm1.020)\times10^6}{T^2} \quad (\mathrm{J\,K^{-1}\,mol^{-1}}) \quad (4)$$

$Bi_7Ta_3O_{18}$

$$C_{pm} = (699.0\pm31.2)+(52.762\pm41.859)\times10^{-3}T - \frac{(9.956\pm1.704)\times10^6}{T^2} \quad (\mathrm{J\,K^{-1}\,mol^{-1}}) \quad (5)$$

Bi_3TaO_7

$$C_{pm} = (251.6\pm14.6)+(67.05\pm19.34)\times10^{-3}T - \frac{(3.237\pm0.799)\times10^6}{T^2} \quad (\mathrm{J\,K^{-1}\,mol^{-1}}) \quad (6)$$

The enthalpy increments as functions of temperature obtained by integration of $C_{\mathrm{pm}}(T)$ (HT fit, Eqs. (4)–(6)) are shown in Fig. 2. The pertinent dependencies deduced from $C_{\mathrm{pm}}(T)$ functions estimated according to the additive Neumann–Kopp's rule (NKR) are given for comparison. Applying NKR [24,25] the heat capacity of complex oxide is calculated as a linear combination of the heat capacities of constituent binary ones. In the case of bismuth tantalum mixed oxide $x(Bi_2O_3).y(Ta_2O_5)$ we can write the following equations:

$$C_{\mathrm{pm}}(x(Bi_2O_3)y(Ta_2O_5)) = xC_{\mathrm{pm}}(Bi_2O_3)+yC_{\mathrm{pm}}(Ta_2O_5) \quad (7)$$

$$\Delta_{\mathrm{ox}}C_{pm} = C_{\mathrm{pm}}(x(Bi_2O_3)y(Ta_2O_5))-xC_{\mathrm{pm}}(Bi_2O_3)-yC_{\mathrm{pm}}(Ta_2O_5) = 0 \quad (8)$$

Temperature dependencies of $\Delta_{\mathrm{ox}}C_{pm}$ for $BiTaO_4$, $Bi_4Ta_2O_{11}$, $Bi_7Ta_3O_{18}$ and Bi_3TaO_7 calculated according to Eq. (8) from experimental C_{pm} data for mixed oxides and literature C_{pm} data

Table 3
Standard thermodynamic functions for bismuth tantalates at 298.15 K.

Oxide	$Bi_4Ta_2O_{11}$	$Bi_7Ta_3O_{18}$	Bi_3TaO_7
$C_{pm}(298.15)$ ($\mathrm{J\,K^{-1}\,mol^{-1}}$)	363.17	602.74	235.16
$H_{\mathrm{m}}(298.15)-H_{\mathrm{m}}(0)$ ($\mathrm{J\,mol^{-1}}$)	66566 ± 384	109760 ± 634	44265 ± 254
$S_{\mathrm{m}}(298.15)$ ($\mathrm{J\,K^{-1}\,mol^{-1}}$)	449.6 ± 2.3	743.0 ± 3.8	304.3 ± 1.6

Table 2
Parameters for the phonon heat capacity.

Oxide	$Bi_4Ta_2O_{11}$			$Bi_7Ta_3O_{18}$			Bi_3TaO_7		
Mode	Θ_i (K)	$10^5\alpha_i$ ($\mathrm{K^{-1}}$)	Degeneracy (n=51)	Θ_i (K)	$10^5\alpha_i$ ($\mathrm{K^{-1}}$)	Degeneracy (n=84)	Θ_i (K)	$10^5\alpha_i$ ($\mathrm{K^{-1}}$)	Degeneracy (n=33)
D	94	5	3	82	8	3	98	5	3
E_1	91	5	6	73	9	8	91	10	4
E_2	202	5	8	154	9	12	235	10	6
E_3	257	9	10	256	12	16	271	15	6
E_4	533	20	10	418	25	20	533	10	8
E_5	759	20	14	820	30	25	899	10	6

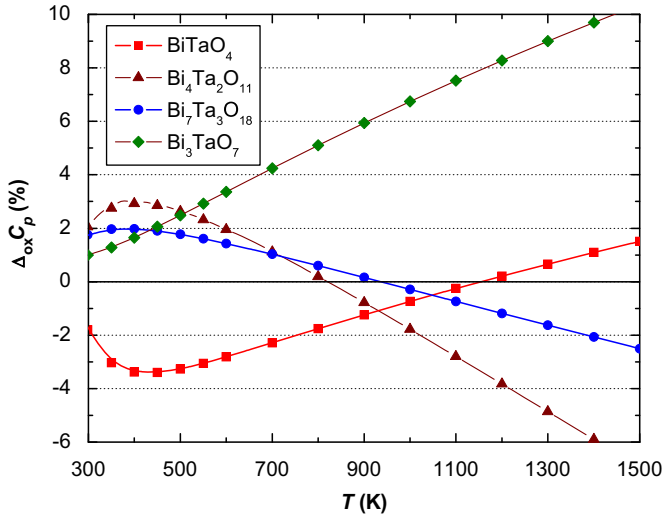

Fig. 3. Temperature dependence of $\Delta_{ox}C_{pm}$ for bismuth tantalum mixed oxides.

for Bi_2O_3 [26] and Ta_2O_5 [27] are shown in Fig. 3. It is obvious that NKR ($\Delta_{ox}C_{pm}=0$) predicts the heat capacities of bismuth tantalum mixed oxides remarkably well around room temperature but in the case of $Bi_4Ta_2O_{11}$ and Bi_3TaO_7 the deviations from NKR become substantial at high temperatures (above approx. 1200 K). Similar behavior was observed previously for strontium and calcium niobates [28–30] and can be explained by differences in dilatation terms due to molar volume contraction or expansion as well as the variation of thermal expansion and compressibility coefficients [25].

The obtained data were included into a thermodynamic database FeRAM [31] compatible with the FactSage software [32] which makes it possible to calculate various phase diagrams in the system $CaO–SrO–Bi_2O_3–Nb_2O_5–Ta_2O_5$.

Acknowledgments

This work was supported by the Czech Science Foundation (Grant no. 104/07/1209) and Ministry of Education of the Czech Republic (research projects No. MSM6046137302 and No. MSM6046137307). The work of P.S. is a part of the research program MSM0021620834 financed by the Ministry of Education of the Czech Republic and was also supported by grant GACR No. P108/10/1006.

Appendix A. Supplementary Material

Supplementary data associated with this article can be found in the online version at doi:10.1016/j.jssc.2010.11.020.

References

[1] W. Zhou, Adv. Mater. 2 (1990) 414.
[2] W. Zhou, J. Solid State Chem. 101 (1992) 1.
[3] C.D. Ling, R.L. Withers, S. Schmidt, J.G. Thompson, J. Solid State Chem. 137 (1998) 42.
[4] C.D. Ling, S. Schmidt, R.L. Withers, J.G. Thompson, N. Ishizawa, S. Kishimoto, Acta Cryst. B55 (1999) 157.
[5] C.D. Ling, J.G. Thompson, R.L. Withers, S. Schmidt, J. Solid State Chem. 142 (1999) 33.
[6] C.D. Ling, J. Solid State Chem. 148 (1999) 380.
[7] I. Abrahams, F. Krok, M. Struzik, J.R. Dygas, Solid State Ionics 179 (2008) 1013.
[8] R.S. Roth, J.L. Waring, Am. Mineralogist 48 (1963) 1348.
[9] C.Y. Lee, R. Macquart, Q. Zhou, B.J. Kennedy, J. Solid State Chem. 174 (2003) 310.
[10] B. Muktha, J. Darriet, G. Madras, T.N. Guru Row, J. Solid State Chem. 179 (2006) 3919.
[11] M. Hampl, A. Strejc, D. Sedmidubský, K. Růžička, J. Hejtmánek, J. Leitner, J. Solid State Chem. 179 (2006) 77.
[12] J.C. Lashley, M.F. Hundley, A. Migliori, J.L. Sarrao, P.G. Pagliuso, T.W. Darling, M. Jaime, J.C. Cooley, W.L. Hults, L. Morales, D.J. Thoma, J.L. Smith, J. Boerio-Goates, B.F. Woodward, G.R. Stewart, R.A. Fisher, N.E. Phillips, Cryogenics 43 (2003) 369.
[13] E. Dachs, C. Bertoldi, Eur. J. Mineral. 17 (2005) 251.
[14] R.A. Marriott, M. Stancescu, C.A. Kennedy, M.A. White, Rev. Sci. Instrum. 77 (2006) 096108.
[15] C.A. Kennedy, M. Stancescu, R.A. Marriott, M.A. White, Cryogenics 47 (2007) 107.
[16] Q. Shi, C.L. Snow, J. Boerio-Goates, B.F. Woodfield, J. Chem. Thermodyn. 42 (2010) 1107.
[17] J.S. Hwang, K.J. Lin, C. Tien, Rev. Sci. Instrum. 68 (1997) 94.
[18] W. Schnelle, J. Engelhardt, E. Gmelin, Cryogenics 39 (1999) 271.
[19] Quantum Design, Physical Property Measurement System – Application Note, 〈http://www.qdusa.com/sitedocs/productBrochures/heatcapacity-he3.pdf〉.
[20] J.W. Arblaster, Platinum Metals Rev. 38 (1994) 119.
[21] J. Rodriguez-Carvajal, Physica B 192 (1993) 55.
[22] C.A. Martin, J. Phys., Condens. Matter 3 (1991) 5967.
[23] W.H. Press, S.A. Teukolsky, W.T. Vetterling, B.P. Flannery, Numerical Recipes in FORTRAN, 2nd Edition, Cambridge University Press, 1992, pp. 402–406.
[24] J. Leitner, P. Chuchvalec, D. Sedmidubský, A. Strejc, P. Abrman, Thermochim. Acta 395 (2003) 27.
[25] J. Leitner, P. Voňka, D. Sedmidubský, P. Svoboda, Thermochim. Acta 497 (2010) 7.
[26] D. Risold, B. Hallstedt, L.J. Gauckler, H.L. Lukas, S.G. Fries, J. Phase Equilib. 16 (1995) 223.
[27] O. Knacke, O. Kubaschewski, K. Hesselmann, Thermochemical Properties of Inorganic Substances, 2nd Ed., Springer, Berlin, 1991.
[28] J. Leitner, I. Šipula, K. Růžička, D. Sedmidubský, P. Svoboda, J. Alloys Compds. 481 (2009) 35.
[29] J. Leitner, K. Růžička, D. Sedmidubský, P. Svoboda, J. J. Thermal Anal. Calorimetry 95 (2009) 397.
[30] J. Leitner, M. Hampl, K. Růžička, M. Straka, D. Sedmidubský, P. Svoboda, Thermochim. Acta 475 (2008) 33.
[31] J. Leitner, D. Sedmidubský, P. Voňka, in: Proceedings of the CALPHAD XXXVIII, 17.–22.5.2009, Prague, Czech Republic, p. 122.
[32] C.W. Bale, P. Chartrand, S.A. Degterov, G. Eriksson, K. Hack, R. Ben Mahfoud, J. Melanqon, A.D. Pelton, S. Petersen, CALPHAD 26 (2002) 189.